Radiolytic Production of Fluorine Gas from MSR Relevant Fluoride Salts

Davis, Lance; Hania, Ralph; Boomstra, Dennis; Rossouw, Dillon; Charpin-Jacobs, Florence; Uhlir, Jan; Maracek, Martin; Beckers, Helmut; Riedel, Sebastian

DOI
10.1080/00295639.2022.2129951

Publication date
2022

Document Version
Final published version

Published in
Nuclear Science and Engineering

Citation (APA)
Davis, L., Hania, R., Boomstra, D., Rossouw, D., Charpin-Jacobs, F., Uhlir, J., Maracek, M., Beckers, H., & Riedel, S. (2022). Radiolytic Production of Fluorine Gas from MSR Relevant Fluoride Salts. *Nuclear Science and Engineering*, *197*(4), 633-646. https://doi.org/10.1080/00295639.2022.2129951

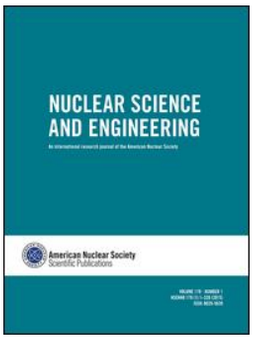

Nuclear Science and Engineering

ISSN: (Print) (Online) Journal homepage: https://www.tandfonline.com/loi/unse20

Radiolytic Production of Fluorine Gas from MSR Relevant Fluoride Salts

Lance Davis, Ralph Hania, Dennis Boomstra, Dillon Rossouw, Florence Charpin-Jacobs, Jan Uhlir, Martin Maracek, Helmut Beckers & Sebastian Riedel

To cite this article: Lance Davis, Ralph Hania, Dennis Boomstra, Dillon Rossouw, Florence Charpin-Jacobs, Jan Uhlir, Martin Maracek, Helmut Beckers & Sebastian Riedel (2022): Radiolytic Production of Fluorine Gas from MSR Relevant Fluoride Salts, Nuclear Science and Engineering, DOI: 10.1080/00295639.2022.2129951

To link to this article: https://doi.org/10.1080/00295639.2022.2129951

NUCLEAR SCIENCE AND ENGINEERING

DOI: https://doi.org/10.1080/00295639.2022.2129951

Radiolytic Production of Fluorine Gas from MSR Relevant Fluoride Salts

Lance Davis,[a,b]* Ralph Hania,[a] Dennis Boomstra,[a] Dillon Rossouw,[a] Florence Charpin-Jacobs,[a] Jan Uhlir,[c] Martin Maracek,[c] Helmut Beckers,[d] and Sebastian Riedel[d]

[a]*Nuclear Research and Consultancy Group (NRG), Westerduinweg 3, NL-1755, LE Petten, The Netherlands*
[b]*Delft University of Technology, Faculty of Applied Sciences, Radiation Science & Technology Department, Mekelweg 15, 2629 JB Delft, The Netherlands*
[c]*Research Centre Rez, Hlavni 130, CZ-250 68, Husinec-Rez, Czech Republic*
[d]*Freie Universität Berlin, Kaiserswerther Str. 16-18, D-14195 Berlin, Germany*

Received June 30, 2022
Accepted for Publication September 19, 2022

Abstract — *Radiolytic fluorine gas production at temperatures of 40°C to 60°C was investigated for the fluoride salts LiF, BeF_2, UF_4, ThF_4, and 71.7LiF-16BeF_2-12.3UF_4 (FliBe-UF_4) by gamma irradiation of powdered samples using spent fuel elements from the High Flux Reactor (HFR) Petten as the irradiation source; work of a similar nature was previously performed at Oak Ridge National Laboratory in the period 1965 to 1995. Gamma irradiation was conducted for just over 41 days, with total absorbed gamma dose ranging from ~45 MGy for the lightest salts to ~170 MGy for ThF_4 and UF_4. By measuring the gas pressure within salt-filled capsules during irradiation, it was possible to quantify radiolytic gas production for all salt samples except UF_4. Production rates are reported as the salt G-values, measured as number of fluorine molecules produced per 100 eV of energy absorbed (molecules F_2/100 eV). The G-values of the salts were found to be G(LiF) ~0.004, G(BeF_2) ~0.009, G(ThF_4) ~0.021, and G(FLiBe-UF_4) ~0.005.*

Keywords — *Gamma radiolysis, molten salt reactor, fluoride salt, nuclear reactor fuel, G-value.*

Note — *Some figures may be in color only in the electronic version.*

I. INTRODUCTION

The molten salt reactor (MSR) is considered a favorable alternative to current mainstay solid fuel nuclear reactor designs (i.e., pressurized water reactors, boiling water reactors) and has received increasing research and development (R&D) attention in the past 10 to 15 years (Refs. 1 through 4), driven by several initiatives to design and realize MSR concepts with varying goals. This recent growth in interest also stems from the recognition of MSRs by the nuclear Generation IV International Forum as one of six promising reactor technologies for further R&D (Refs. 1 and 3).

MSRs offer numerous advantages when compared to traditional solid fuel reactor designs, with the specific draws being their ability to operate at significantly higher temperatures (representing increased efficiency and higher value heat) and lower operating pressures (representing a lower driving force behind the spreading of activity and reduced loads on containment structures), as well as passive safety features and the potential to strongly reduce both fuel consumption and waste production.[5] However, significant challenges related to qualification of MSR fuels and materials exist due to the requirements of high operating temperatures, intense neutron radiation, and representative corrosive environment.

Radiolysis, the phenomenon of relevance in this work, is the chemical bond cleaving effect induced by

*E-mail: davis@nrg.eu

ionizing radiation occurring in molecular materials and salts, including the halide salts intended for use in MSRs. The conventional description of radiation-induced damage in halide salt crystals starts with a primary process that involves creation of interstitials (H-centers) and vacancies (F-centers) in the halide sublattice,[2,6–8] referred to as primary defects, with an insignificant effect on the cation sublattice.[9,10] Complex intermediate processes follow (described in detail elsewhere[11]), leading to a late stage in which extended defects are created in the form of metallic colloidal precipitates and atomic or molecular halogen (bubbles), by aggregation of F-centers and H-centers, respectively.[6,7,10,12] The halogen bubbles are able to coalesce and diffuse to the grain boundaries of the salt through a similar mechanism as that of dislocation loop punching, observed for gases in irradiated metals,[11,13,14] and escape from the crystal surface. Additionally, as the halide salt is subjected to progressive radiation damage, interactions between primary and extended defects lead to the formation and growth of vacancy voids.[7,8] In Ref. 15, a mechanism is proposed in which the halogen bubbles/gas in irradiated halide salt are/is expected to grow to a stable size at relatively low irradiation dose, whereas vacancy voids grow in a progressive logarithmic manner with increasing irradiation dose.[7,15] As the vacancy voids grow within the salt crystal, they collide with the finely dispersed halogen bubbles, absorbing the halogen bubbles and filling the void with halogen gas. When the dimensions of the gas-filled vacancy voids exceed the mean distance between metallic colloids and halogen bubbles (gas) in the crystal lattice, the halogen gas and metallic colloids interact within the vacancy void resulting in a powerful recombination reaction.[8] It should be stated that this overview of the halide salt radiolysis process is largely based on studies of alkali halide salts, and although the overall process is expected to be similar for divalent (and higher valency) halide salts due to the lesser role of the cation sublattice, there are notable deviations, particularly in the intermediate radiolysis stages. These deviations/differences are discussed in other work.[16–18]

In 2019, the Nuclear Research & Consultancy Group (NRG) completed the 2-year irradiation campaign of SALIENT-01 (Ref. 19), a fluoride molten salt fuel irradiation experiment in the High Flux Reactor (HFR). The SALIENT-01 experiment contained four 78LiF-22ThF_4 salt samples in graphite crucibles; the main topics for investigation were fission product speciation and relocation, interaction of the fuel salt with moderator graphite, and spent fuel salt processing. During the preparation of SALIENT-01, radiolytic production of corrosive fluorine (F_2) gas from the fluoride salt was identified as both an operational and an experiment risk, based on the preceding work[20–22] on fluoride salt irradiation conducted by Oak Ridge National Laboratory (ORNL) during the 1960s within the Molten Salt Reactor Experiment (MSRE) program.

Follow-up experimental work[23] on fuel salt radiolysis was conducted by ORNL in the mid-1990s with specific focus on the now stored spent fuel salt, which was used in the MSRE during its operation. These ORNL experiments had shown appreciable quantities of fluorine gas produced from fluoride salts when subjected to gamma and/or beta radiation fields below temperatures of 70°C to 150°C. Fluorine production was also shown[23] to be dependent on the state/nature of the salt (composition, granularity, and grain size) and the rate of energy deposition into the fluoride salt.

In fuel irradiation experiments, low sample temperatures are realized during reactor downtime for routine refueling unless the samples can be heated externally. In MSRs the low salt temperatures may generally be avoided, but understanding and quantifying the radiolytic production of F_2(g) is still of importance for future safety and licensing aspects (i.e., spent fuel salt storage, handling of fuel salt leaks, fuel salt behavior during postincident and accident scenarios, etc.) associated with the use of fluoride-based fuel salts in MSRs.

Thus, in a collaboration with Research Center Rez (CVR) and Freie Universität Berlin (FUB), NRG has set out to reproduce and expand on past experimental measurements of F_2(g) production under gamma irradiation within the SAlt GAmma (SAGA) experimental project. This contribution focuses on the description of the experiment and the determination of radiolytic F_2(g) production efficiencies (G-values) at close to room temperature.

II. EXPERIMENTAL

II.A. Sample Preparation

The five halide salt samples specified in Table I and produced at CVR were inserted into the SAGA facility for gamma irradiation using the spent fuel from the HFR as the gamma source. The BeF_2 and LiF samples were prepared from pure (> 99.95% and 99.98% purity, respectively) batches of BeF_2 and LiF purchased from Shanghai Muhong Industrial Company, Ltd. The UF_4 and ThF_4 samples were obtained from batches synthesized at CVR and found to be > 99.95% pure through X-ray diffraction analysis; however, differential scanning calorimetry

TABLE I

Samples Irradiated in the SAGA Experimental Facility

Capsule	Sample	Physical Form	Mass (g)
1	BeF_2	Fine powder	6.0 ± 0.1
2	LiF	Fine powder	8.5 ± 0.1
3	He (empty reference)		
4	71.7LiF-16BeF_2-12.3UF_4	Fine powder	13.9 ± 0.1
5	UF_4	Fine powder	14.1 ± 0.1
6	ThF_4	Fine powder	12.4 ± 0.1

measurements indicated the presence of trace UF_3 in the UF_4 samples. The LiF-BeF_2-UF_4 sample, prepared from the aforementioned salt sample batches, was molten, solidified, and ground to a fine powder, producing mixed crystals.

These salt samples were placed in gas-tight, pre-fluorinated Monel-400 capsules (see Fig. 1), of 100-mm height and 9-mm inner diameter, connected to pressure sensors (model PNA161, EFE sensors) using VCR connectors, as shown in Fig. 2. Prior to fluorination, all components were cleaned with a solution of 0.2% Galvaclean-20 in an ultrasonic bath, rinsed with deionized water, cleaned with ethanol, and then finally dried in air. Thereafter, possibly developed oxide layers were removed from the inside walls of the capsules by contacting, dissolving, and rinsing the capsules with 0.5% HF solution (pH 1.6) for approximately 3 to 4 min. The components were then rinsed again with deionized water and dried in an argon atmosphere glove box. Fluorination of the inside of the capsules at > 150°C was performed at FUB and subsequently repeated at CVR. Upon completion of the fluorination, the salt samples were loaded into the capsules, after which the capsules were sealed inside a helium atmosphere glove box. The connection of the capsules to the calibrated pressure sensors was made through 50-cm-long minitubes. The minitubes are required to distance and shield the pressure sensors from the strong gamma field at the salt sample position. The calculated internal volume of the capsules including the minitubes and connection to the calibrated pressure sensors was 8.4 ± 0.2 cm^3.

Each capsule, providing the first containment, was then placed into a second containment that was then sealed. To capture any fluorine gas that may escape the first containment in the event of accidental capsule failure, 22 g of HTC™ NI 600 RP (Johnson-Matthey) activated catalyst of high nickel surface area on an alumina substrate was placed in each of the second containments.[24] This catalyst was activated by reduction under 95%Ar-5%H_2 at 275°C for 6 h. The plenum space in the second containment was 175.5 cm^3 (excluding addition of the capture catalyst). The five salt-filled capsules and one He-filled capsule were then placed together in an aluminum capsule holder of the larger, complete SAGA facility, which provided the third containment barrier, as shown in Figs. 2 and 3. The SAGA facility

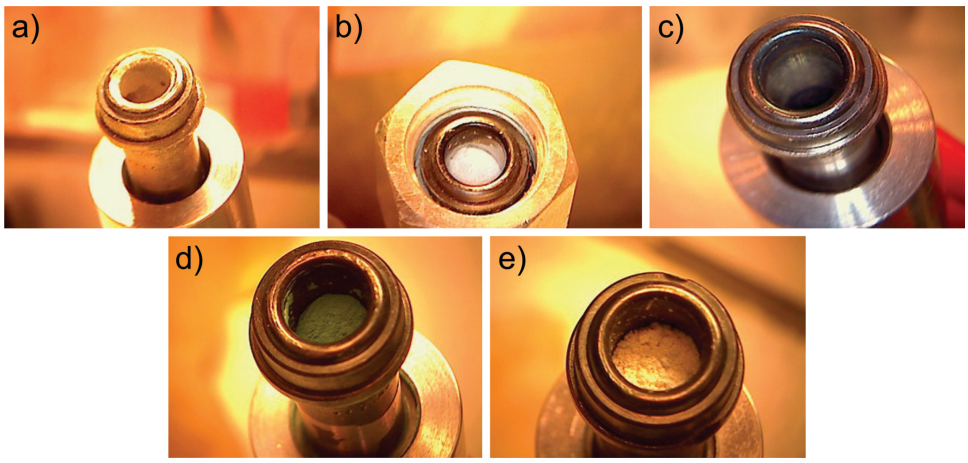

Fig. 1. Salt-containing capsules: (a) BeF_2, (b) LiF, (c) FLiBe-UF_4, (d) UF_4, and (e) ThF_4.

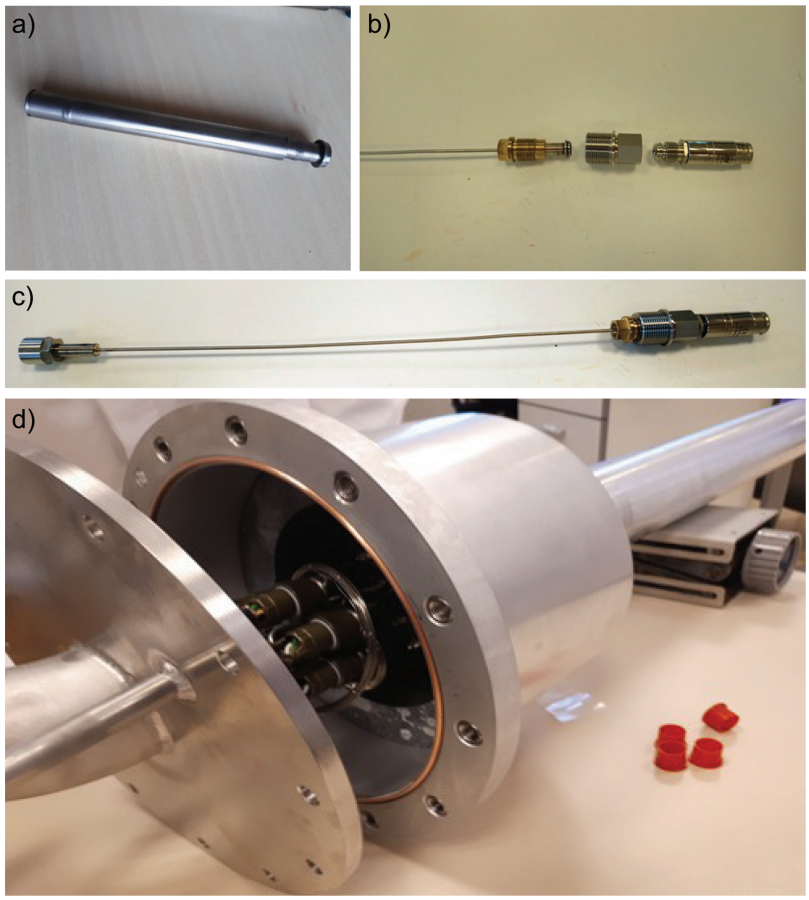

Fig. 2. SAGA assembly components: (a) salt capsule first containment, (b) pressure sensor connection to salt capsule through a minitube, (c) minitube assembly, and (d) assembled SAGA capsule array inserted into third containment.

was filled with N_2 gas with a total plenum volume of 3.5 L.

II.B. GAMMA IRRADIATION SOURCE

The SAGA facility containing the salt samples was placed in a central position surrounded by eight spent fuel elements in the HFR spent fuel rack (SFR) and was irradiated in this configuration, as shown in Fig. 4. In aiming to reach a point of equilibrium of fluorine gas production and adsorption/recombination in a reasonable timescale, estimated to occur at a total absorbed dose of around 200 MGy (Refs. 20, 21, 22, and 25) but depending on the sample, spent fuel elements with the highest burnup and shortest cooling time were used.

The eight spent fuel elements used can be divided into two fuel types: Type-1 (F1) is a spent fuel element coming from the most recent HFR cycle, and type-2 (F_2) is a fuel element from the previous HFR cycle with an additional decay time of 35 to 40 days. This fuel usage scheme ensured the highest possible gamma dose rates to the salt samples during the irradiation period.

III. IRRADIATION

III.A. Pressure and Temperature Measurements

Pressure and temperature measurements from the five salt capsules were taken at time intervals of 1 min and recorded/logged by the HFR Data Acquisition System (DACOS). The pressure measurements recorded during the irradiation period are shown in Fig. 5. When subjected to gamma irradiation, all salt samples besides UF_4 exhibited a pressure increase of varying magnitude from their ~1-bar starting pressure. As seen in Fig. 5, the pressure increase is strongest for the ThF_4 sample, and in addition, the pressure for this sample already increases before the start of irradiation. This reveals a nonnegligible gamma dose rate in the wider vicinity of the SFR, which cannot be easily avoided.

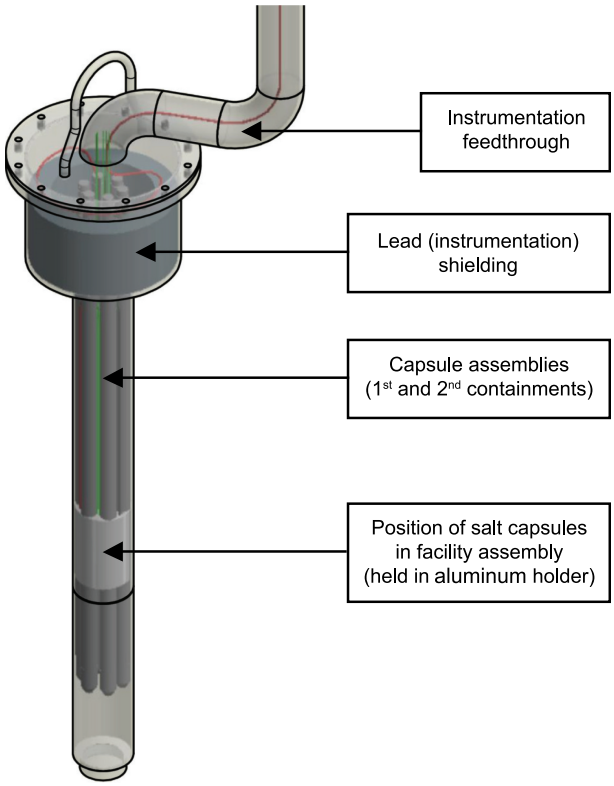

Fig. 3. Assembled SAGA experimental facility.

The pressure development in the UF_4 is difficult to account for: A < 1-bar capsule pressure was recorded at loading, while a prompt increase to 1.85 bars was observed before the start of irradiation, and a hyperbolic pressure development was observed during irradiation. The UF_4 pressure data were therefore considered unusable. It is not clear whether these deviations from expectation are due to errors related to the experimental equipment used, i.e., capsule sealing, pressure sensors, data acquisition system, and/or a combination of one or more of these factors. Additionally, it is considered noteworthy that unlike the other cations present in the salt samples, uranium can change its oxidation state,[26,27] which may influence the energetics and kinetics of the excited states in the crystal and thus its behavior during radiolysis. One effect that has been observed in MSRE spent fuel salt is the formation of UF_6(g) through the reaction of radiolytic F_2 with UF_4 in the salt.[22,23]

The SAGA facility was removed from its irradiation position in the SFR on two occasions: the first removal period, which lasted 1653 min, and the second removal period, which lasted 54 min, indicated by points b to c and d to e in Figs. 5 and 6, respectively. During these removal periods, the facility was lifted to a temporary storage position above and away from the SFR but remained within the HFR pool. It was not expected that these short breaks in irradiation would have noticeable effects on the pressure measured in the capsule, as pressure increases are related to the F_2 production via radiolysis of the fluoride salt and only minor temperature reductions (3°C maximum) were observed on the sample capsule surface during the removal periods compared to the 40°C to 42°C irradiation temperature (Fig. 6). Although the measured temperatures as shown in Fig. 6

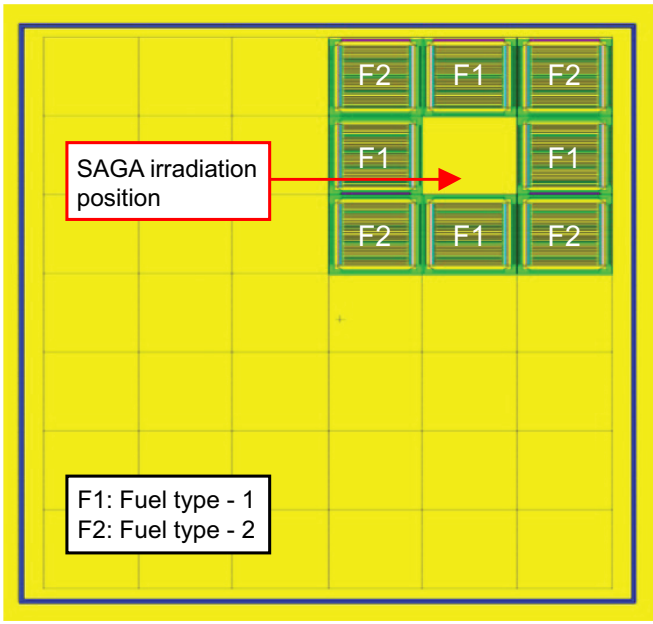

Fig. 4. SAGA experimental facility irradiation position.

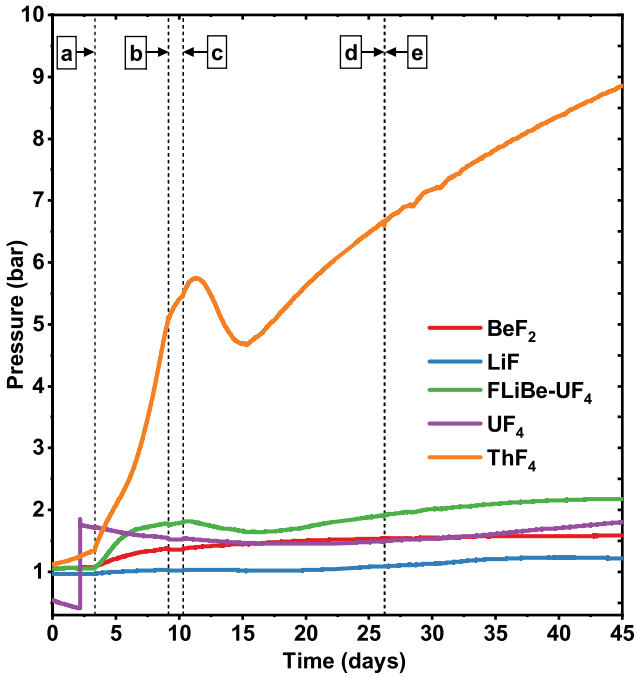

Fig. 5. SAGA salt capsule pressure measurements. Point a: SAGA beginning of irradiation, point b: SAGA out of irradiation, point c: SAGA in irradiation, point d: SAGA out of irradiation, and point e: SAGA in irradiation.

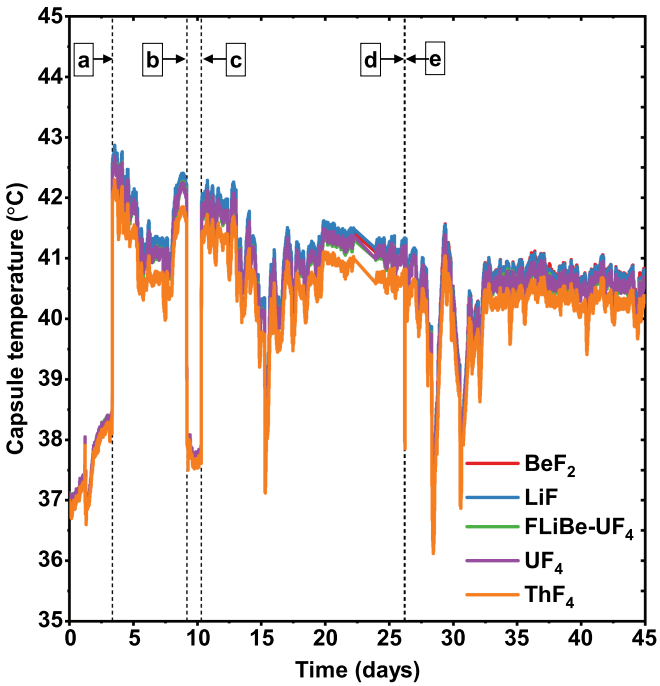

Fig. 6. SAGA salt capsule temperature measurements. Point a: SAGA beginning of irradiation, point b: SAGA out of irradiation, point c: SAGA in irradiation, point d: SAGA out of irradiation, and point e: SAGA in irradiation.

are those of the sample capsules, based on thermal calculations it is expected that the maximum salt temperatures are < 9°C higher than the measured capsule temperatures and thus too low for significant recombination to occur (i.e., > 150°C) (Ref. 25).

These expectations appear to hold for BeF_2 but not for the other salts, which appear to exhibit an anomalous trend following the first removal period, as shown in Fig. 5 (after point c) and Figs. 9 through 12. The reason for this anomalous trend is currently unclear. It is postulated that this pattern indicating a pressure decrease and recovery may be due to the complex radiation damage accumulation and extended defect creation mechanisms in the halide salt matrices, perhaps in combination with hydraulic (mechanical) shock experienced by the samples when lifting the facility out of its irradiation position.

III.B. QUANTIFICATION OF GAMMA FIELD

During the SAGA irradiation period in 2019, three gamma dose rate measurements were made at the sample location to quantify the gamma field: before and after the experiment, and in between two irradiation periods. However, considering the poor statistics of these measurements, an additional measurement campaign was conducted during the period of September to November 2021 to better characterize the gamma profile of the spent fuel irradiation array. For ease of reference, the 2019 and 2021 gamma dose measurements are hereinafter distinguished as GM-19 and GM-21, respectively.

Gamma dose rate measurements were conducted by inserting an air-filled gamma ionization chamber into the central SAGA irradiation position in the SFR (Fig. 4) and measuring the gamma dose at a number of elevations over the total height of the irradiation position. The position-dependent gamma dose measurements were then converted to overall sample dose rates by mean-value integration of each measurement set (of a given day) over the height of the sample. By conducting these gamma measurements over an extended period, a time-evolved dose rate profile is generated, as measured during the GM-19 and GM-21 campaigns. Supplementary information pertaining to these gamma measurements is provided online.

To further refine the gamma dose rate profile, the dose rate curves provided by the GM-19 and GM-21 measurements were curve fitted (exponential decay fit) and linearly interpolated to produce an average gamma dose rate curve for the SAGA irradiation, as shown in Fig. 7.

Since the irradiation of the SAGA facility only commenced ~19 days after the end of the HFR operational

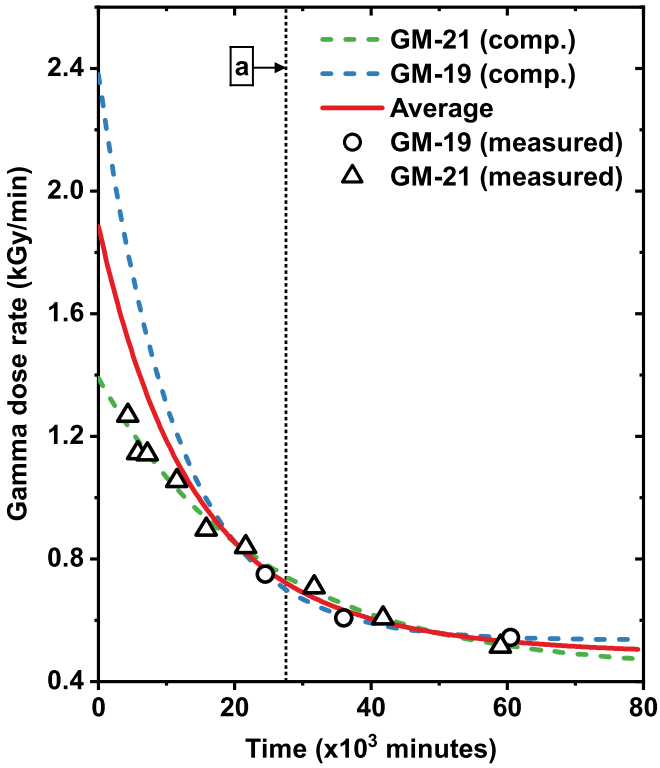

Fig. 7. Gamma dose rate (in air) versus time after fuel discharge, as determined from two sets of ionization chamber measurements. Point a: start of the SAGA irradiation.

cycle, the characteristic equation of the average gamma dose rate curve is time-adjusted to account for the exact period elapsed between the end of the HFR cycle and the beginning of SAGA irradiation (27 540 min), given by $D_R[\mathrm{kGy/min}] = (13.56)\exp((-t+27540)/14652.63)-+0.51$. The derivation process used for obtaining this time-adjusted average gamma dose rate equation is provided as supplementary information which is available online. The approximate maximum uncertainty in this average curve is taken as ~3.5%, determined from the mean of the maximum noted deviation between the computed GM-19 and GM-21 curves from $t > 27\,450$ min (insertion of SAGA into irradiation position).

IV. EXPERIMENTAL DATA PROCESSING

To convert the pressure measurements obtained for each salt capsule throughout the irradiation period to F_2 production quantities, the following calculation routine was used:

Step 1: The pressure measurements recorded for each salt capsule were temperature corrected using the ideal gas equation of state (EOS), thereby obtaining the time-evolved F_2 quantity in moles corresponding to each pressure-temperature data point. In doing so, minor pressure deviations due to temperature fluctuations are dampened/normalized. The use of the ideal gas EOS is considered a reasonable approximation to relate experimental pressures and temperatures as F_2 exhibits near ideal behavior (compressibility factor Z ~1) at SAGA experimental conditions (i.e., pressure 1 to 10 bars, temperature 30°C to 50°C) (Refs. 28 and 29).

Step 2: The F_2 production in each salt capsule (in mmol) is then divided by the mass of the salt inserted into the given capsule, giving F_2 per gram salt (mmol F_2/g salt).

Step 3: The salt capsule pressure measurements (converted to mmol/g salt) were assessed for the time period before $t = 0$ (SAGA beginning of irradiation) to obtain a background/baseline reading for each salt capsule.

Step 4: The baseline determined in step 3 is then subtracted from each measurement point (mmol/g) over the complete irradiation time period, producing normalized F_2 production values.

To determine the F_2 production efficiencies (G-values), the F_2 production curves should furthermore be expressed in terms of dose absorbed by the salt samples. To accomplish this, first the gamma emission spectrum of the spent fuel elements was determined by simulating the complete history of the elements in the HFR core using a combination of MCNP4C3 (Ref. 30) and FISPACT-2007 (Ref. 31) calculations to determine fuel burnup and composition. This photon spectrum was implemented as the irradiation source, which allows for computation of the time-dependent dose rates in the salt and He capsules. An MCNP calculation routine was then employed to determine the effective time-dependent energy deposition in the salt samples, with particular attention being paid to the spatial distribution of the gamma field inside the SAGA facility. This was done by first developing an MCNP model of the experimental geometry and materials, as shown in Fig. 8.

A geometrical model was also made for the air-filled ionization chamber measurements, allowing for a direct relation between physical gamma dose measurements with an air-filled ionization chamber and the computed dose rates in the samples. The computed dose rates for the various salts are then divided by the computed dose rates in the ionization chamber to obtain dose rate factors for the salts. These factors are provided in Table II; statistical uncertainties for these factors are < 2%.

By applying the dose rate factor for the given salt, the cumulative absorbed dose (throughout the duration of the

TABLE II

Sample Dose Rate Factors Relative to the Ionization Chamber Air Reference

Capsule	Sample	Dose Rate Factor
1	BeF_2	0.796
2	LiF	0.793
3	He	0.850
4	71.7LiF-16BeF_2-12.3UF_4	2.124
5	UF_4	2.909
6	ThF_4	2.889
—	Air (reference)	1.000

SAGA irradiation) can be converted to absorbed dose per gram salt (in Wh/g).

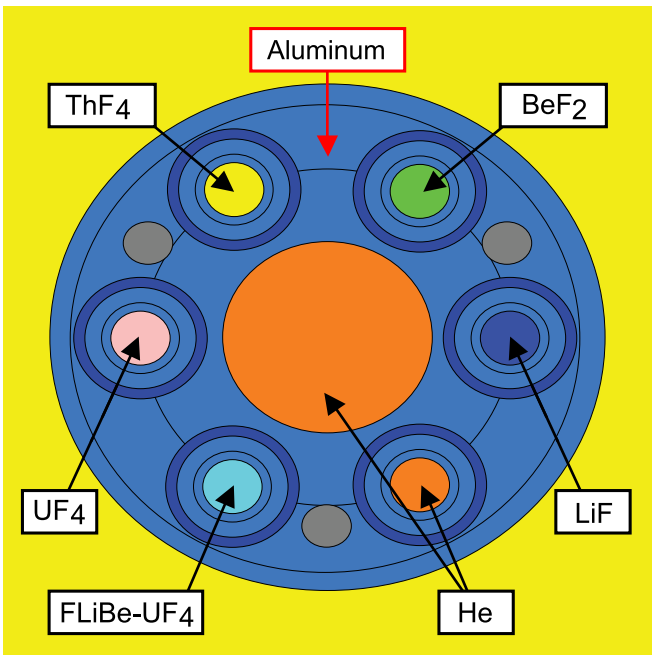

Fig. 8. Top view of SAGA sample holder in MCNP model geometry.

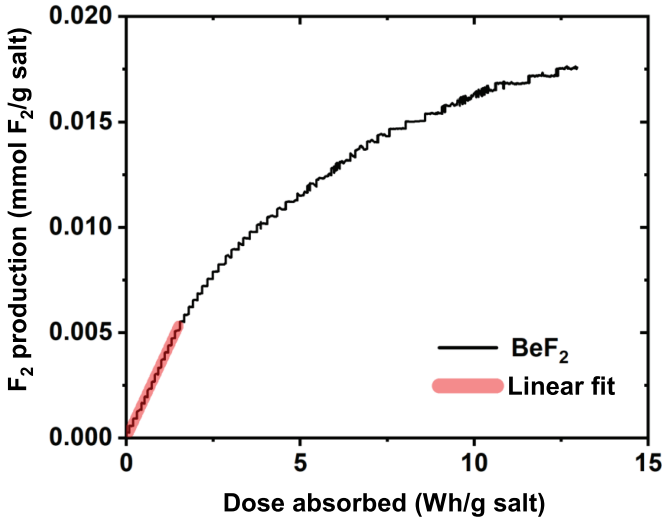

Fig. 9. BeF_2 fluorine production curve.

V. RESULTS AND DISCUSSION

The F_2 production curves for the five fluoride salts irradiated in SAGA are shown in Figs. 9 through 12. As discussed in Sec. III.A pertaining to the correlation between the observed pressure decrease and recovery pattern and the brief removal of the SAGA facility from irradiation, F_2 production curves are far from the expected near-exponential shape except in the case of BeF_2. This phenomenon does warrant future consideration but does not render the determination of F_2 production efficiencies invalid.

It is assumed here that the pressures produced in the capsules are only due to the production of F_2(g). Minor pressure contributions from radiolytically produced trace gases (e.g., O_2, H_2O, HF) from impurities present in the salt matrices and/or secondary reactions [e.g., $F_2 + UF_4 \rightarrow UF6(g)$] cannot be excluded with absolute certainty. Mass spectrometry of evolved gases is planned for future gamma irradiations. However, considering the reported purity of the salts and handling processes during the salt capsule filling, it is not expected that the pressure contribution of trace gases would be significant.

The F_2 production efficiency (in molecules F_2 per 100 eV of energy deposited), also referred to as the G-value, can be obtained by measuring the slope of the linear-increasing portion of the F_2 production curve.[22] The measured slope can be expressed as a G-value using a unit conversion factor of 2.68, which is the ratio of 6.022E20 F_2 molecules (per 1 F_2 mmol) over (2.247E20) × 100 eV (per 1 Wh).

V.A. BeF_2

The F_2 production curve obtained for the BeF_2 salt sample resembles an upward exponential decay shape, as shown in Fig. 9. The maximum G-value for the BeF_2 was found to be ~0.009 molecules F_2/100 eV, with this maximum occurring as expected in the early (initial) stages of gamma absorption. It is not clear from the experimental data if the BeF_2 reaches the F_2 production plateau (equilibrium), as the irradiation ends before the tail end of the

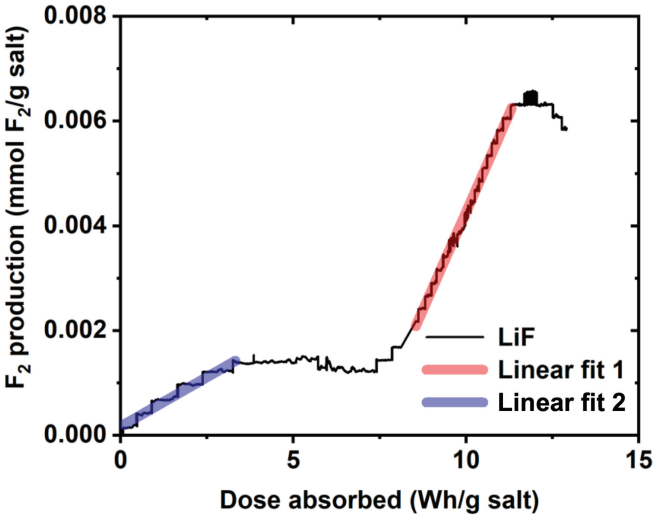

Fig. 10. LiF fluorine production curve.

data set could be resolved. It does however appear that at the end of irradiation, BeF_2 was approaching a F_2 production plateau as the production slope appears to be flattening around 12.5 Wh/g salt (45 MGy) absorbed dose.

V.B. LiF

The LiF production curve, shown in Fig. 10, exhibits two distinct linear regions: One region is an initial slope at the start of irradiation, and the other is a maximum production slope occurring after absorbing a dose of ~8 Wh/g salt (28.8 MGy). The initial linear F_2 production is interrupted by a period exhibiting a production plateau after an absorbed dose of about 3.5 Wh/g salt, which is directly following an interruption of the irradiation (Sec. III.A). The plateau period continues until an absorbed dose of 8 Wh/g salt, leading to a strong linear increase in F_2 production. This period of maximum production continues up until an absorbed dose of ~11.4 Wh/g salt (41.04 MGy) before the production flattens, followed by a pressure decrease beyond an absorbed dose of 12.5 Wh/g salt.

It is not clear why the LiF exhibits these two distinct F_2 production regions. One postulate considered is that the first (and longest) removal period of the SAGA facility from its irradiation position may have induced mechanical/hydraulic shock to the LiF salt crystals, which favors the recombination (back) reaction, leading to a period of minimal F_2 production, which is followed by the resumption of strong F_2 production as higher cumulative energy absorption occurs within the salt.

Thus, for completeness, F_2 production efficiencies (G-values) for LiF of both the initial production slope and the maximum production slope were reported and were found to be ~0.001 and ~0.004 molecules F_2 /100 eV, respectively. Although no directly comparable experimental work reporting a G-value for LiF can be found in literature, ORNL conducted an irradiation of LiF using soft X-rays with a maximum dose rate of 0.3 kGy/h (Ref. 32). That experimental work reports no F_2 production during irradiation. Considering the low dose rate during X-ray irradiation in that ORNL work, the absence of observed F_2 production/liberation is not a completely unexpected result.

V.C. FLiBe-UF_4

Similarly to the LiF (and ThF_4) sample, the FLiBe-UF_4 salt sample appears to have been affected by the removal and reinsertion of the SAGA facility during the irradiation period. As seen from the FLiBe-UF_4 production curve in Fig. 11, this removal and reinsertion point is noticeable from the vertical increase around 10.3 Wh/g salt, after which the mentioned F_2 production decrease and recovery occur, followed by what seems to be an approach to equilibrium. Because of the uncertainties introduced by this handling action and the lack of a detailed model of the process, the F_2 production curve beyond this vertical increase is not assessed further.

For this FLiBe-UF_4 data set, the maximum F_2 production (maximum slope) does appear to occur in the early stages of irradiation and is thus not influenced by the handling error. A maximum F_2 production efficiency

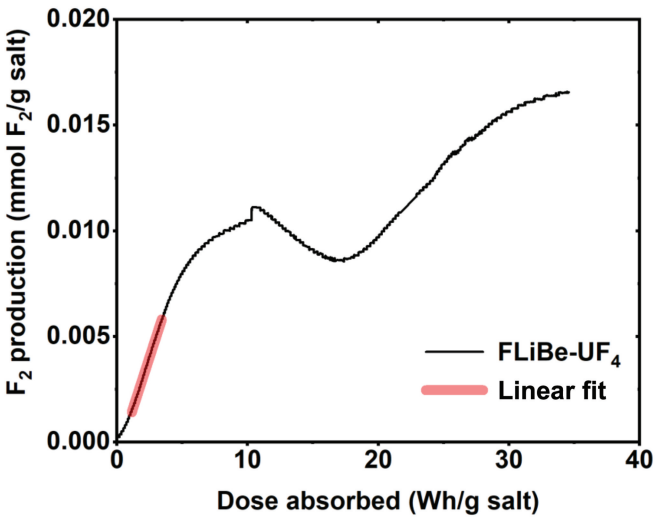

Fig. 11. FLiBe-UF_4 fluorine production curve.

(G-value) of ~0.005 molecules F_2/100 eV is reported for the FLiBe-UF_4 salt.

In experimental studies conducted by ORNL (Refs. 23 and 32) and more recently the Kurchatov Institute[33] (KI), F_2 production efficiencies (G-values) for a number of similar mixed salts to that of the FLiBe-UF_4 (71.7LiF-16BeF_2-12.3UF_4) irradiated in this work have been reported. The results from these experimental studies show significant scatter and are not directly comparable to the FLiBe-UF_4 irradiation in this work, as the salt compositions (and particle sizes) vary. However, the G-values reported in these studies for similar mixed salts range from 0.005 to 0.045, and thus, the FLiBe-UF_4 G-value in this work does fall within the lower end of this wide range.

V.D. ThF_4

The removal and reinsertion point for the ThF_4 can be seen in Fig. 12 from the vertical increase around 14 Wh/g salt, after which the previously discussed F_2 production decrease and recovery occur. The system is clearly still far from equilibrium at the end of irradiation.

The ThF_4 production curve prior to the handling activity discussed above exhibits two regions of linear F_2 production: One is an initial slope, and the other (maximum slope) occurs prior to the facility removal activity. F_2 production efficiencies (G-values) for ThF_4 of both the initial and maximum production slopes were reported and were found to be ~0.007 and ~0.021 molecules F_2/100 eV, respectively. No directly comparable experimental gamma radiolysis work on ThF_4 has been published in current literature. However, an ORNL experiment[32] in which ThF_4 was subjected to soft-X-ray irradiation at a maximum dose rate of 2.9 kGy/h reported a G-value of 0.005 molecules F_2/100 eV.

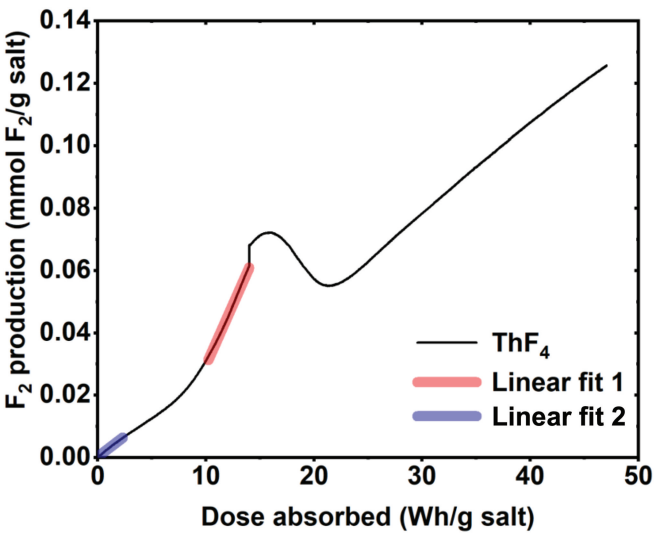

Fig. 12. ThF_4 fluorine production curve.

V.E. Evaluation of F_2 Production Efficiencies

From the F_2 production curves for the four irradiated salts (UF_4 not reported), G-values were obtained and are provided in Table III together with relevant literature values.

Looking at Table III, no literature value is available for comparison for BeF_2, and the absence of F_2 production reported previously for LiF may be explained on account of the relatively low dose rate applied. For FLiBe salt mixtures, the highest G-value reported in literature[21] was for that of the MSRE (ORNL) salt, which was a LiF-BeF_2-ZrF_4-UF_4 eutectic, reported to be 0.045 molecules F_2/100 eV. However, G-values in the range of 0.01 to 0.02 were reported to be typical from supplementary studies[23] of this MSRE salt. Notwithstanding the current variance and uncertainties associated with radiolytic F_2 production efficiencies of fluoride salts, the G-values obtained from the SAGA experiment appear to be within the bounds of expectation for the salt samples investigated, with the current measurement for FLiBe-UF_4 on the low end and for ThF_4 on the high end of the range.

In short, results reported for MSR relevant fluoride salts (Table III) show significant scatter. The scatter is thought to be caused by differences in physical form (grains versus fused ingots), grain sizes, sample temperatures, and potential measurement errors.

An additional factor that may contribute to the variance in reported G-values is the presence of cation impurities in the salt matrix. It is well established that cation impurities act as H-center traps at low temperatures[34] and subdue vacancy void growth,[7] both suppressive effects in terms of halogen gas formation and release. Salt impurities are thus of marked relevance, as purity information of salts in MSR-related radiolysis experiments[23,32,33] is not consistently given, and high levels of cation impurities may result in an underestimation of the reported G-value for a given pure salt matrix. An interesting consequence would be that as fuel salts are used within an MSR, through which impurity levels are expected to increase due to corrosion and fission processes, the resulting spent fuel in its frozen state would be less sensitive to radiolytic halogen production and release.

TABLE III

F_2 Production Efficiencies (G-Values) Obtained for Salts Irradiated in This Work and a Number of Comparable Salts Reported in Literature.

Salt Type	Salt Form	G-Value (Molecules F_2/100 eV)		Irradiation Source	Maximum Dose Rate (kGy/h)	Conducted by
		This Work	Literature			
BeF_2	Fine powder	0.009		HFR Fuel	33	NRG
LiF	Fine powder	0.004		HFR Fuel	33	NRG
	Not reported		0	Soft X-rays	0.3	ORNL (Ref. 32)
71.7LiF-16BeF_2-12.3UF_4	Fine powder	0.005		HFR Fuel	89	NRG
65LiF-29BeF_2-5ZrF_4-0.66UF_4	Solid plug		0.005 to 0.031	Post irradiation energy	Not reported	ORNL (Ref. 23)
	Solid plug		0.045	^{60}Co source	6.3	ORNL (Ref. 23)
	Powder		0.012	HFR Fuel	175.4	ORNL (Ref. 23)
	Fine powder		0.005 to 0.04	Soft X-rays	1.3	ORNL (Ref. 32)
71.7LiF-16BeF_2-12ThF_4-0.3UF_4	Solid plug		0.006	In-core test	Not reported	KI (Ref. 33)
66LiF-33BeF_2-1UF_4	Solid plug		0.01	In-core test	Not reported	KI (Ref. 33)
ThF_4	Fine powder	0.021		HFR Fuel	121	NRG
	Not reported		0.003 to 0.008	Soft X-rays	2.9	ORNL (Ref. 32)

It has been qualitatively reported[35,36] that the radiation stability of (pure) inorganic salts is influenced by a number of factors such as bonding nature, ionization energy, lattice free volume, and nature/type of defects induced by radiation damage. Radiation stability, which is a measure of a substance's ability to withstand radiation-induced structural changes, can be taken as an inverse measure of radiation yield. Thus, under the same irradiation conditions, salts with lower radiation stability are expected to yield greater quantities of radiolytic products.

From the BeF_2 and LiF G-values reported in this work, it appears that BeF_2 has a significantly higher (more than double) F_2 production efficiency. In Ref. 37 it is proposed that in radiolysis processes in which the primary defect production occurs within the halide (anion) sublattice, the overall efficiency of salt decomposition is proportional to the electron affinity of the primary defect products. It has been reported[18,38] that halide salts of divalent cations, such as BeF_2, produce charged defect pairs (anionic vacancies and interstitial halides) in the halide sublattice when irradiated, as opposed to neutral primary defects produced by alkali halide salts. Thus, through this mechanism, BeF_2 producing defects with greater electron affinity would be expected to produce greater radiolysis yields (higher G-value) as that of LiF.

Furthermore, in Refs. 35 and 39, a correlation is made between radiolysis yield from an ionic salt and the free volume of the salt's lattice. The free volume is defined as the difference between the lattice unit cell volume and the ions occupying the unit cell, representing the interactive behavior of the bonds in the ionic salt.[39] The radiation-damaged sublattice is typically less strongly bound in salt crystals with larger free volumes; thus, the probability for diffusion and release of radiolysis products (i.e., halogen gas) from the salt crystal is higher.[35] The lattice parameters (a, b, c, α, β, γ) of BeF_2 and LiF lattices are (4.739 Å,

4.739 Å, 5.1875 Å, 90 °, 90 °, 120 °) and (4.027 Å, 4.0247 Å, 4.027 Å, 90 °, 90 °, 90 °) (Ref. 40), respectively. Using these lattice parameters as a measure of free volume, it can be seen that BeF_2 is expected to have a greater free volume than LiF and thus by this measure should release greater quantities of radiolysis products [i.e., F_2(g)] compared to that of LiF. Therefore, notwithstanding other variables and uncertainties (i.e., grain sizes, differences in impurity type and quantities), both the nature (charged) of the primary defects produced in irradiated BeF_2 and the larger free volume of the BeF_2 lattice may be (qualitatively) contributory effects explaining the higher G-value observed for BeF_2 as opposed to LiF.

Some radiolysis experiments of this nature have reported delay of fluorine production at the start of the salt irradiation, termed "induction period."[25] This induction period is thought to be related to a complementary effect of accumulation of fluorine gas within the crystal lattice of the salt and the diffusion rate of halide gas toward the salt crystal surface.[22,36] However, these induction periods are not consistently noted in fluoride salt radiolysis experiments, and they are absent in this work.

Finally, it appears that the observed production decrease and recovery following the movement of the SAGA facility out of and back into the radiation field are more significant for the heavier salts (FLiBe-UF_4 and ThF_4) compared to LiF. This may be related to higher accumulated radiation damage (due to higher gamma absorption) in the heavier salts in the time period up to the first facility removal operation. For the halide sublattice of the heavier salts, the number of primary defects (F-center and H-center), extended defects (metallic colloids and halogen bubbles), and associated vacancy voids within the salt crystal at the time of the facility movement would be higher than that of the lighter salts. Since vacancy void growth is proportional to dose absorbed,[7] the vacancy voids are expected to be larger in the heavier salt. The combined effect of higher number density and larger dimensions of extended defects (specifically metallic colloids) and larger vacancy voids increases the significance of the recombination back reaction, which may explain the observed pressure decrease of the heavier salt samples upon removal from the gamma field. In addition, the F_2 production curves for the heavier FLiBe-UF_4 (Fig. 11) and ThF_4 (Fig. 12) salts indicate a marked F_2 increase around the period during which the SAGA facility was removed from the gamma field. In Refs. 41 and 42, it is shown that the recombination reaction between metallic colloids and halogen gas filled vacancy voids is significantly energetic, leading to a very rapid temperature and pressure increase within the vacancy void. This may provide a complementary/partial explanation for the observed F_2 increase (spike) preceding the F_2 production decrease. It is noteworthy to mention that a similar observation was made in ORNL work[21] following an interruption of (^{60}Co) gamma irradiation of MSRE fuel salt.

VI. CONCLUSIONS AND RECOMMENDATIONS

Powdered samples of the fluoride salts LiF, BeF_2, UF_4, ThF_4, and 71.7LiF-16BeF_2-12.3UF_4 (FliBe-UF_4) were subjected to gamma radiation from spent fuel elements of the HFR Petten, and pressure increase was measured to obtain information on radiolytic fluorine gas production for these samples. Pressure development observed for UF_4 cannot be easily explained and may be due to a defective sensor. The absence of a clear pressure increase may also be related to the existence of multiple valence states for uranium, although the most likely effect of this would be the formation of UF_6(g) (Refs. 22 and 23), which was not observed during post irradiation heating of the samples to above the boiling point.

For the other samples, the maximum production rates, measured as the number of fluorine molecules produced per 100 eV of energy absorbed (molecules F_2/100 eV), were found to be G(LiF) ~0.004, G(BeF_2) ~0.009, G(ThF_4) ~0.021, and G(FLiBe-UF_4) ~0.005. The LiF, ThF_4, and FLiBe-UF_4 samples showed a complex pressure response to movement (and assumed combinatory effects of mechanical shock and salt crystal lattice defect mechanisms) of the irradiation facility around the spent fuel pool.

A follow-up SAGA irradiation campaign will be conducted in order to verify and refine the G-values reported for these fluoride salts and the factors that influence them. The following changes are made to the experiment to improve measurements and scope:

1. When repeating the gamma irradiation, the facility should not be moved or disturbed during the irradiation period.

2. The irradiation period will be extended in order to verify the existence of equilibria between production and adsorption/recombination.

3. One or more chloride salts will be added to the experiment to obtain information on chloride radiolysis (NaCl, KCl, or a heavy chloride) since radiolytic gas

production data on chloride salts are even more limited than for fluoride salts.

Acknowledgments

This work is supported by the Dutch Ministry of Economic Affairs.

Disclosure Statement

No potential conflict of interest was reported by the author(s).

Supplementary Material

Supplemental data for this article can be accessed online at https://doi.org/10.1080/00295639.2022.2129951.

ORCID

Lance Davis http://orcid.org/0000-0003-3401-6660
Ralph Hania http://orcid.org/0000-0003-2550-6270

References

1. H. KAMIDE et al., "Generation IV International Forum-GIF," Annual Report 2020 INIS-FR-21-0718, Organisation for Economic Co-operation and Development (2021).
2. T. DOLAN, *Molten Salt Reactors and Thorium Energy*, Woodhead Publishing Series in Energy, Elsevier Science (2017).
3. D. LEBLANC, "Molten Salt Reactors: A New Beginning for an Old Idea," *Nucl. Eng. Des.*, **240**, *6*, 1644 (2010);); https://doi.org/10.1016/j.nucengdes.2009.12.033.
4. J. SERP et al., "The Molten Salt Reactor (MSR) in Generation IV: Overview and Perspectives," *Prog. Nucl. Energy*, **77**, 308 (2014)); https://doi.org/10.1016/j.pnucene.2014.02.014.
5. H. MACPHERSON, "Molten-Salt Reactors," *Proc. Int. Conf. Constructive Uses of Atomic Energy*, Washington, D.C., 1968.
6. Y. EKMANIS, "Radiolysis Behaviour in Alkali Halide Crystals," *Nucl. Instrum. Methods Phys. Res. Sect. B*, **1**, *2–3*, 473 (1984); https://doi.org/10.1016/0168-583X(84)90111-3.
7. V. DUBINKO et al., "Modeling of the Radiation-Induced Microstructural Evolution in Ionic Crystals," *Nucl. Instrum. Methods Phys. Res. Sect. B*. **153**, *1–4*, 163 (1999); https://doi.org/10.1016/S0168-583X(99)00043-9.
8. V. DUBINKO et al., "Theory of the Late Stage of Radiolysis of Alkali Halides," *J. Nucl. Mater.*, **277**, *2–3*, 184 (2000); https://doi.org/10.1016/S0022-3115(99)00207-X.
9. A. LIDIARD, "The Radiolysis of Alkali Halides—The Nucleation and Growth of Aggregates," *Z. Phys. Chem.*, **206**, *1–2*, 219 (1998); https://doi.org/10.1524/zpch.1998.206.Part12.219.
10. A. TURKIN et al., "Radiolysis of NaCl at High and Low Temperatures: Development of Size Distribution of Bubbles and Colloids," *J. Phys.: Condens. Matter*, **18**, *24*, 5655 (2006); https://doi.org/10.1088/0953-8984/18/24/007.
11. C. CATLOW, K. DILLER, and L. HOBBS, "Irradiation-Induced Defects in Alkali Halide Crystals," *Philos. Mag. A*, **42**, *2*, 123 (1980); https://doi.org/10.1080/01418618009365806.
12. V. DUBINKO et al., "New Mechanism for Radiation Defect Production and Aggregation in Crystalline Ceramics," *J. Nucl. Mater.*, **289**, *1–2*, 86 (2001); https://doi.org/10.1016/S0022-3115(00)00686-3.
13. V. DUBINKO et al., "A New Mechanism for Radiation Damage Processes in Alkali Halides," *J. Appl. Phys.*, **86**, *11*, 5957 (1999); https://doi.org/10.1063/1.371639.
14. N. GAO et al., "Loop-Punching Suppression Induced by Growth of Helium Bubble Pair in Tungsten," *J. Appl. Phys.*, **124**, *23*, 235105 (2018); https://doi.org/10.1063/1.5053138.
15. V. DUBINKO, D. VAINSHTEIN, and H. DEN HARTOG, "Mechanism of Void Growth in Irradiated NaCl Based on Exiton-Induced Formation of Divacancies at Dislocations," *Nucl. Instrum. Methods Phys. Res. Sect. B*, **228**, *1–4*, 304 (2005); https://doi.org/10.1016/j.nimb.2004.10.061.
16. P. CALL, W. HAYES, and M. KABLER, "Optical Detection of Exciton EPR in Fluorite Crystals," *J. Phys. C: Solid State Phys.*, **8**, *4*, L60 (1975); https://doi.org/10.1088/0022-3719/8/4/006.
17. A. EGRANOV et al., "Radiation Defects in CaF_2 and SrF_2 Crystals Doped with Cadmium or Zinc," *J. Phys.: Condens. Matter*, **20**, *46*, 465213 (2008); https://doi.org/10.1088/0953-8984/20/46/465213.
18. A. RAMOS-BALLESTEROS et al., "Gamma Radiation-Induced Defects in KCl, $MgCl_2$, and $ZnCl_2$ Salts at Room Temperature," *Phys. Chem. Chem. Phys.*, **23**, *17*, 10384 (2021); https://doi.org/10.1039/D1CP00520K.
19. P. HANIA et al., "SaLIENT-01: Preparation and Start of Irradiation of Thorium-Bearing Molten Fluoride Salt in Graphite Crucibles," *Proc. Int. Nuclear Fuel Cycle Conf. and TOP FUEL 2019—Light Water Reactor Fuel Performance Conf. 2020*, Seattle, Washington,

September 22–27, 2019, p. 285, American Nuclear Society (2020).

20. M. ROSENTHAL, R. BRIGGS, and P. KASTEN, "Molten-Salt Reactor Program Semiannual Progress Report for Period Ending February 28, 1969," ORNL-4396, Oak Ridge National Laboratory (1969).
21. P. HAUBENREICH, "Fluorine Production and Recombination in Frozen MSR Salts After Reactor Operation." ORNL-TM-3144, Oak Ridge National Laboratory (1970).
22. A. ICENHOUR et al., "An Overview of Radiolysis Studies for the Molten Salt Reactor Remediation Project," *Proc. Int. Conf. Global 2001*, Paris, France, September 9–13, 2001.
23. D. WILLIAMS, G. D. CUL, and L. TOTH, "A Descriptive Model of the Molten Salt Reactor Experiment After Shutdown: Review of FY 1995 Progress," ORNL/TM-13142, Oak Ridge National Laboratory (1996).
24. D. WILLIAMS and J. BRYNESTAD, "Evaluation of Fluorine-Trapping Agents for Use During Storage of the MSRE Fuel Salt," ORNL/TM-13770, Oak Ridge National Laboratory (1999).
25. L. TOTH and L. FELKER, "Fluorine Generation by Gamma Radiolysis of a Fluoride Salt Mixture," *Radiat. Eff. Defects Solids*, **112**, *4*, 201 (1990); https://doi.org/10.1080/10420159008213046.
26. K. KVASHNINA et al., "Chemical State of Complex Uranium Oxides," *Phys. Rev. Lett.*, **111**, *25*, 253002 (2013); https://doi.org/10.1103/PhysRevLett.111.253002.
27. G. LEINDERS et al., "Evolution of the Uranium Chemical State in Mixed-Valence Oxides," *Inorg.Chem.*, **56**, *12*, 6784 (2017); https://doi.org/10.1021/acs.inorgchem.7b01001.
28. K. DE REUCK, "Fluorine International Thermodynamic Tables of the Fluid State," Vol-11, IUPAC Chemical Data Series No. 36, International Union of Pure and Applied Chemistry (1990).
29. H. ESLAMI and A. BOUSHEHRI, "The Equation of State of Song and Mason Applied to Fluorine," *Int. J. Thermophys.*, **20**, *2*, 611 (1999); https://doi.org/10.1023/A:1022665323146.
30. "MCNP™—A General Monte Carlo N-Particle Transport Code," J. F. BRIESMEISTER, Ed., Version 4C, LA-13709-M, Los Alamos National Laboratory (2000).
31. R. FORREST, "FISPACT-2007: User Manual," UKAEA-FUS-534, UKAEA Fusion Association (2007).
32. R. BRIGGS, "Molten-Salt Reactor Program Semiannual Progress Report for Period Ending July 31, 1964," ORNL-3708, Oak Ridge National Laboratory (1964).
33. V. IGNATIEV, "Molten Salts Characteristics Under Irradiation in Fission Related Systems," IAEA-TECDOC 1912, p. 70, International Atomic Energy Agency (2020).
34. E. KOTOMIN, M. ZAISER, and W. SOPPE, "A Mesoscopic Approach to Radiation-Induced Defect Aggregation in Alkali Halides Stimulated by the Elastic Interaction of Mobile Frenkel Defects," *Philos. Mag. A*, **70**, *2*, 313 (1994); https://doi.org/10.1080/01418619408243187.
35. V. V. GROMOV, "Effect of Impurities on Radiation-Chemical Processes in Crystals of Inorganic Salts," *Russian Chem. Rev.*, **43**, *2*, 79 (1974); https://doi.org/10.1070/RC1974v043n02ABEH001791.
36. A. ICENHOUR, "Radiolytic Effects on Fluoride Impurities in a U_3O_8 Matrix," ORNL/TM-2000/157, Oak Ridge National Laboratory (2000).
37. V. BOLDYREV and L. BYSTRYKH, "The Chemical Action of Ionising Radiations on Inorganic Crystals," *Russian Chem. Rev.*, **32**, *8*, 426 (1963); https://doi.org/10.1070/RC1963v032n08ABEH001352.
38. C. B. LUSHCHIK, I. VITOL, and M. ELANGO, "Decay of Electronic Excitations into Radiation Defects in Ionic Crystals," *Sov. Phys. Usp.*, **20**, *6*, 489 (1977); https://doi.org/10.1070/PU1977v020n06ABEH005405.
39. G. BOYD, E. W. GRAHAM, and Q. LARSON, "Recoil Reactions High Intensity Slow Neutron Sources. IV. The Radiolysis of Crystalline Alkali Metal Bromates with γ-Rays," *J. Phys Chem.*, **66**, *2*, 300 (1962); https://doi.org/10.1021/j100808a026.
40. L. MEI et al., "Investigation of Thermal Neutron Scattering Data for BeF_2 and LiF Crystals," *J. Nucl. Sci. Technol.*, **50**, *4*, 419 (2013); https://doi.org/10.1080/00223131.2013.773169.
41. D. VAINSHTEIN et al., "Effect of the Void Formation on the Explosive Fracture of Electron Irradiated NaCl Crystals," *Nucl. Instrum. Methods Phys. Res. Sect. B*, **166**, 550 (2000); https://doi.org/10.1016/S0168-583X(99)00717-X.
42. A. TURKIN, et al., "Kinetics of Back Reaction Between Radiolytic Products Initiated by Radiation-Induced Voids in NaCl," *J. Phys.: Condens. Matter.*, **13**, *1*, 203 (2001); https://doi.org/10.1088/0953-8984/13/1/321.